Communication

In silico discovery of new dopants for Fe-doped Ni oxyhydroxide (Ni1-xFexOOH) catalysts for oxygen evolution reaction

Hyeyoung Shin, Hai Xiao, and William A. Goddard

J. Am. Chem. Soc., **Just Accepted Manuscript** • DOI: 10.1021/jacs.8b02225 • Publication Date (Web): 11 May 2018

In silico discovery of new dopants for Fe-doped Ni oxyhydroxide ($Ni_{1-x}Fe_xOOH$) catalysts for oxygen evolution reaction

Hyeyoung Shin, Hai Xiao, and William A. Goddard III*

Materials and Process Simulation Center (MSC) and Joint Center for Artificial Photosynthesis (JCAP), California Institute of Technology, Pasadena, California 91125, USA

Supporting Information Placeholder

ABSTRACT: The oxygen evolution reaction (OER) is critical to efficient water splitting to produce the H_2 fuel for sustainable energy production. Currently, the best non-noble metal OER electrocatalyst in base conditions is the Fe-doped NiOOH ($Ni_{1-x}Fe_xOOH$), with η=0.4, but much lower values are desired. We use density functional theory to determine the overall mechanism for the OER of $Ni_{1-x}Fe_xOOH$, concluding that promoting radical character on the metal−oxo bond is critical to efficient OER. Then we consider replacing Fe with 17 other transition metals of the Fe, Ru, and Os rows, where we find 3 new promising candidates: Co, Rh, and Ir, which we predict to have η=0.27, 0.15, and 0.02, respectively, all very much improved performance compared to Fe, making all three systems excellent candidates for experimental testing.

Artificial photosynthesis (AP) to split water into H_2 and O_2 could provide renewable sustainable energy production. However, critical challenge in AP for water splitting is to develop highly active electrocatalysts that reduce the overpotential for the oxygen evolution reaction (OER)[1].

The current most active non-noble electrocatalysts for OER under alkaline condition are the Fe-doped Ni oxyhydroxides ($Ni_{1-x}Fe_xOOH$), which are far more efficient than NiOOH,[2-4] but still not adequate. To design better catalysts, we need first to determine the reaction mechanism explaining why Fe doping improves OER efficiency. Some studies argue that Fe sites are the active site,[3-5] whereas other studies suggest that Ni sites are the active sites for OER on $Ni_{1-x}Fe_xOOH$.[6,7]

Here we use density functional theory (DFT) calculations to determine the energy barriers and required applied potential for each of the steps involved in OER. Unlike the previous DFT studies, [3,8] we built realistic models that explicitly include both intercalated species and the aqueous environment under OER operation conditions, and performed DFT calculations to reveal the origin of the unusual high OER activity of $Ni_{1-x}Fe_xOOH$ and to provide guidance for designing electrocatalysts with higher activity.

We find that in $Ni_{1-x}Fe_xOOH$ both Fe^{4+} and Ni^{4+} play essential roles in the OER by promoting an active site with radical character on the O of a metal-oxo (MO) bond (the role of high spin d^4 Fe) and providing the site for favorable O-O bond coupling (the role of low spin d^6 Ni), so that Fe^{4+} and Ni^{4+} function as co-catalysts. This is why $Ni_{1-x}Fe_xOOH$ leads to a much lower overpotential and better catalytic activity for OER compared to NiOOH.

Based on this new understanding of the mechanism, we then carry out *in silico* QM studies to find new promising OER catalysts. We examine 17 other transition metals in the +4 oxidation state to find ones that could promote MO radical character. We find just three new candidates: Co, Rh, or Ir doped NiOOH to improve the OER over $Ni_{1-x}Fe_xOOH$.

We perform spin-polarized DFT calculations using the VASP[9] to determine the atomistic mechanisms and to find the key factors contributing to improvement in the performance for OER on $Ni_{1-x}Fe_xOOH$. We use the PBE exchange–correlation functional[10], which has been applied successfully to determine a variety of reaction mechanisms.[11-14] For simulation details, see Supporting Information (SI).)

γ-NiOOH is known to be the active phase of NiOOH for OER.[2,3] It includes intercalated species (K^+ ions and H_2O molecules) unlike other phases, but there is no crystal structure. So we use the structure of γ-NiOOH proposed by Ceder.[15] (Figure S1) This structure is consistent with the P3 oxygen stacking sequence and an average Ni oxidation state of +3.66 from experiments.

In our model, we add one water monolayer (three H_2O) on the surface of the NiOOH slab model to explicitly consider how water molecules are involved in the overall OER process. We find that two H_2O's strongly bind on Ni^{4+} sites. One is adsorbed as H_2O but the other is dissociatively adsorbed with OH on a neighboring Ni^{4+} site and H added to the bridging O between Ni^{4+} and Ni^{3+}. A third H_2O molecule does not bind on the

remaining Ni^{3+} site because the unpaired electron on the d_{z2} of Ni^{3+} repels the lone pairs of H_2O molecule (unlike Ni^{4+} with an empty d_{z2}). (Figure 1a)

To achieve a fundamental understanding of the origin of high OER activity in $Ni_{1-x}Fe_xOOH$, we first investigated the lowest free energy pathways for OER on NiOOH. We considered all possible intermediates and reaction states for OER, which proceeds through sequential oxidation steps (losing one electron for each step) coupled with deprotonation. Each oxidation-deprotonation step was systematically explored by comparing the energies required to remove one H atom from the surface for all possible deprotonation sites.

As shown in Figure 2, the entire OER pathways on NiOOH consist of the six reaction steps (four oxidation-deprotonation steps and two non-electrochemical steps);

(1) From **State 1** (Figure 1a), the first oxidation takes place with deprotonation of the hydrogen bonded to the bridging O between Ni^{3+} and Ni^{4+} and with the Ni^{3+} hydroxylated and oxidized to Ni^{4} from the neighboring H_2O that did not chemosorb on the surface. (**State 2**) This step requires 1.21 eV.

(2) The second oxidation step proceeds with deprotonation of the H_2O adsorbed on a neighboring Ni^{4+} as shown in **State 3**. This step requires 0.81 eV and leads to two chemisorbed OH's.

(3) The third oxidation step generates an O species via deprotonation of the OH adsorbed on Ni^{4+} with one additional H_2O introduced as in **State 4**. This oxidation step is endothermic by 2.06 eV, the largest over the entire OER process. Analysis of the DFT spins shows that this O has radical character, with a spin population of 0.58, leading to Ni^{4+}–O•. This O radical (O•) formation step determines the onset potential so that O• formation is the key intermediate in OER, but it is not stabilized sufficiently on the Ni^{4+}.

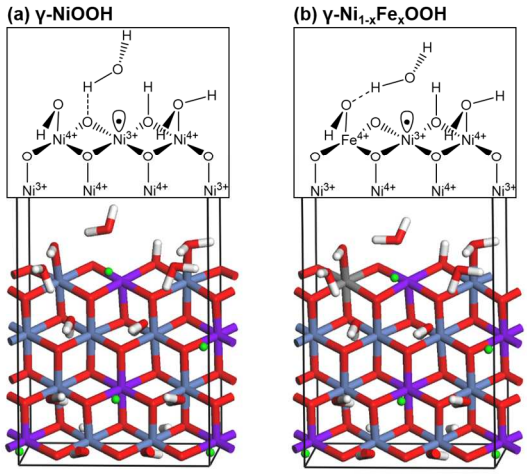

Figure 1. Models for NiOOH and $Ni_{1-x}Fe_xOOH$ OER electrocatalysts. (100) slab models with one explicit water layer for (a) γ-NiOOH and (b) γ-$Ni_{1-x}Fe_xOOH$. Blue, purple, red, white, green and gray atoms indicate Ni^{4+}, Ni^{3+}, O, H, K^+, and Fe^{4+}, respectively. Chemical structures for each model surface are shown as insets. (Note that the intercalating K^+ and H_2O are not shown in the insets for clarity.)

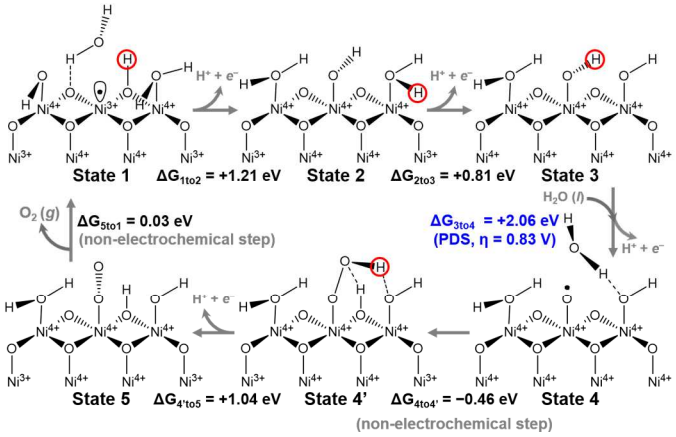

Figure 2. Mechanism for OER on NiOOH catalyst leading to η = 0.83 V.

(4) In **State 4'** the O• from **State 4** promotes O–O coupling to solvent H_2O to form OOH adsorbed on Ni^{4+}. Consequently, the bridging O between Ni^{4+} sites is hydrogenated. This step is exothermic by 0.46 eV. Note that the role of O• in promoting O-O coupling is not an electrochemical step.

(5) **State 4'** undergoes the fourth oxidation step with deprotonation of the OOH, requiring 1.04 eV and generating superoxide (O_2^-) with a bond distance of 1.31 Å as shown in **State 5**. **State 5** goes back to the starting point (**State 1**) after releasing O_2 molecule (uphill by 0.03 eV). The O_2 is released through a non-electrochemical charge transfer step. (O_2^- + $Ni^{4+} \rightarrow O_2$ (g) + Ni^{3+})

Consequently, the Potential Determining Step (PDS) for OER on the NiOOH is the O• generation step, requiring 2.06 eV free energy. We estimate the overpotential (η) by subtracting the thermodynamic equilibrium potential (1.23 V for OER) from the highest free energy required for OER. This leads to η=0.83 V (2.06-1.23), which is comparable to the experimental value of ~0.7 V for OER on γ-NiOOH.[3]

For the case of $Ni_{1-x}Fe_xOOH$, we first searched six different plausible dopant sites on NiOOH as shown in Figure S2. We found that Fe prefers to substitute the Ni^{4+} that interacts with surface OH (> 0.3 eV more stable than other sites), leading to the Fe^{4+} oxidation state. There have been previous reports about the existence of Fe^{4+} and Ni^{4+} in $Ni_{1-x}Fe_xOOH$ under OER operation condition,[4,5,7] in agreement with our predictions in Figure 1b.

Starting with **State 1** (Figure 1b), we investigated the OER mechanism on $Ni_{1-x}Fe_xOOH$ just as for NiOOH, finding that Fe incorporation into the NiOOH dramatically changes the pathways and energetics involved in OER, as shown in Figure 3.

The first oxidation-deprotonation step leads to **State 2** (endothermic by 1.17 eV, similar to that of NiOOH),

while the second and third oxidation steps occur with sequential deprotonation of the adsorbed H_2O on Fe^{4+} in $Ni_{1-x}Fe_xOOH$ (unlike the case of NiOOH) (see **State 3** and **State 4**), requiring 0.70 eV and 1.68 eV, respectively. We note that the key O• intermediate forms on the surface Fe^{4+} site, reducing the energy required for the PDS step to 1.68 eV because the high spin d^4 Fe^{4+} site stabilizes the unpaired electron of the O• thereby reducing the energy cost for the step. The O-O coupling is achieved by interaction of the O• with an additional H_2O introduced at the third oxidation step, leaving the bridging O between Ni^{4+} sites hydrogenated.

However, **the O-O coupling prefers to occur at the low spin d^6 Ni^{4+} rather than at high spin d^4 Fe^{4+}.** The OOH formation on Ni^{4+} (**State 4'-Ni**) leads to O-O coupling (endothermic by 0.01 eV) while O-O coupling on Fe^{4+} (**State 4'-Fe**) is endothermic by 0.41 eV. **This indicates that both Fe^{4+} and Ni^{4+} play essential bifunctional roles in the OER catalysis.**

Next, the fourth oxidation takes place with deprotonation of the OOH adsorbed on Ni^{4+} to form O_2^- (with bond distance of 1.29 Å) on the Ni^{4+}. (**State 5**, endothermic by 1.09 eV) This is consistent with surface enhanced Raman spectroscopy by Koper[16] implicating ($NiOO^-$) superoxide species in $Ni_{1-x}Fe_xOOH$. Then O_2 (g) is released from **State 5** and the surface state goes back to the original **State 1** by an endothermic process (0.04 eV).

These DFT results show that in $Ni_{1-x}Fe_xOOH$ the O• formation is the PDS, as in NiOOH, however, η is much reduced to 0.45 V (1.68-1.23), compared to that of NiOOH (η=0.83 V), which is consistent with the experimental value of ~0.4 V in $Ni_{1-x}Fe_xOOH$.[3] Thus the beneficial effects of Fe incorporation into NiOOH is stabilizing the key intermediate, O•, thereby lowering the η and increasing the electrocatalytic activity for OER.

Now we understand the bifunctional nature of the catalysis in the $Ni_{1-x}Fe_xOOH$ for OER with both Ni and Fe essential for high OER activity. Here the high spin d^4 Fe^{4+} site facilitates formation of the key O• intermediate, while the closed shell d^6 Ni^{4+} site stabilizes O-O

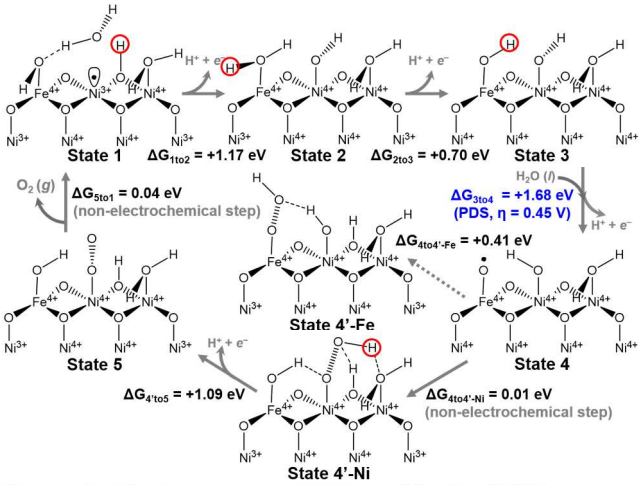

Figure 3. Mechanism for OER on $Ni_{1-x}Fe_xOOH$ catalyst leading to η = 0.45 V.

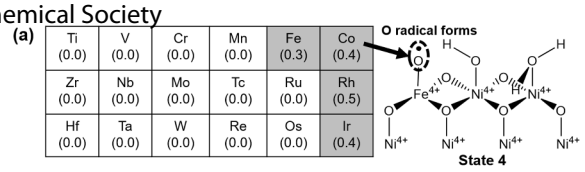

(b)

(eV)	bare NiOOH	Fe-doped	Co-doped	Rh-doped	Ir-doped
ΔG_{1to2}	1.21	1.17	1.11	1.16	**1.25**
ΔG_{2to3}	0.81	0.70	0.98	0.93	0.59
ΔG_{3to4}	**2.06**	**1.68**	**1.50**	**1.38**	1.12
$\Delta G_{4to4'-Ni}$	-0.46	0.01	0.10	0.25	0.70
$\Delta G_{4to4'-Fe}$	-	0.41	0.40	0.55	0.97
$\Delta G_{4'to5}$	1.04	1.09	0.71	0.71	0.76
ΔG_{5to1}	0.03	0.04	0.30	0.25	0.28
η (V)	0.83	0.45	0.27	0.15	0.02

Figure 4. *In silico* screening results for transition metal (TM) doped NiOOH catalysts. (a) The spin density (in parentheses) of O on the MO bond for all 18 TM elements. The four dopants showing O radical on the MO bond are highlighted. (Fe, Co, Rh, and Ir) (b) Free energies involved in the OER process for these best 4 dopants, as in Figure 3. The free energy required for PDS of each material is highlighted in bold and η is summarized in the bottom line.

coupling, the key step for releasing O_2 as the final product. These calculations explain why $Ni_{1-x}Fe_xOOH$ has better OER activity than NiOOH.

Next, we will use these findings to search for new dopant elements to replace the Fe in stabilizing the O• character on the MO bond. Thus, we consider the group 4 to 9 transition metals (TM) from the Fe, Ru, and Os rows (17 elements, in addition to Fe) as dopants on NiOOH, testing how they change the energetics involved in OER.

Since O• character is essential for O−O coupling, [17,18] we optimized the structures corresponding to **State 4** of $Ni_{1-x}Fe_xOOH$ by substituting surface Fe with each of these 17 TMs. Using spin population analysis, we identified that in addition to Fe only three cases have O• on the dopant site with oxidation state of +4. (see Figure 4a). These are the group 9 TM elements (Co, Rh, and Ir).

Next, we performed geometry optimization for all six steps in the OER pathways of $Ni_{1-x}Fe_xOOH$ after substituting Fe with Co, Rh, or Ir. As summarized in Figure 4b, we found that the free energy required to generate the key intermediate, O•, is reduced even more than for Fe, by 0.18, 0.30 , and 0.56 eV when Co, Rh, or Ir are incorporated into NiOOH instead of Fe (see ΔG_{3to4} in Figure 4b). However, the O-O coupling step still prefers to take a place on Ni^{4+} site not on the Co^{4+}, Rh^{4+} or Ir^{4+} dopant sites, just as for $Ni_{1-x}Fe_xOOH$. This suggests that **the group 9 TM-doped NiOOHs are promising electocatalysts for OER,** leading to the same bifunctional catalysis as for $Ni_{1-x}Fe_xOOH$ by stabilizing the O•. For Co and Rh-doped NiOOHs, the PDS is the O• formation as the cases of NiOOH and $Ni_{1-x}Fe_xOOH$, but the overpotentials are reduced to 0.27 V and 0.15 V, respectively. However, for Ir-doped NiOOH, the first oxidation step is the PDS, reducing the overpotential to 0.02 V. These results suggest that Co, Rh, and Ir-doped NiOOH might

be efficient electrocatalysts for OER, probably better than $Ni_{1-x}Fe_xOOH$. We suggest that these dopants should be tested for OER experimentally.

Summarizing, we used DFT to determine the atomistic mechanisms for OER on $Ni_{1-x}Fe_xOOH$, finding that Fe^{4+} and Ni^{4+} both play essential role on OER in $Ni_{1-x}Fe_xOOH$; with high spin d^4 Fe^{4+} stabilizing the O• formation on the MO bond, while the subsequent O-O coupling is catalyzed on low spin d^6 Ni^{4+} making $Ni_{1-x}Fe_xOOH$ a much better OER catalyst than NiOOH where O• is not sufficiently stabilized. Thus, the Fe^{4+} and Ni^{4+} sites co-catalysts lead to optimal OER performance. Then, we carried out *in silico* screening for OER electrocatalysis for doping of γ-NiOOH by other TMs. We predict that Co, Rh and Ir doped NiOOH also stabilize the key intermediate, O• and that they should lead to even lower overpotential than Fe.

ASSOCIATED CONTENT

Supporting Information. Detailed information regarding the geometries and the dopant site search (PDF) The Supporting Information is available free of charge on the ACS Publications website

AUTHOR INFORMATION

Corresponding Author

***wag@wag.caltech.edu**

ACKNOWLEDGMENT

This work was supported by the JCAP, a DOE Energy Innovation Hub, supported through the Office of Science of the U.S. Department of Energy under Award No. DE-SC0004993.

REFERENCES

(1) Walter, M. G.; Warren, E. L.; McKone, J. R.; Boettcher, S. W.; Mi, Q. X.; Santori, E. A.; Lewis, N. S. *Chem Rev* **2010**, *110*, 6446.

(2) Trotochaud, L.; Young, S. L.; Ranney, J. K.; Boettcher, S. W. *J Am Chem Soc* **2014**, *136*, 6744.

(3) Friebel, D.; Louie, M. W.; Bajdich, M.; Sanwald, K. E.; Cai, Y.; Wise, A. M.; Cheng, M. J.; Sokaras, D.; Weng, T. C.; Alonso-Mori, R.; Davis, R. C.; Bargar, J. R.; Norskov, J. K.; Nilsson, A.; Bell, A. T. *J Am Chem Soc* **2015**, *137*, 1305.

(4) Ahn, H. S.; Bard, A. J. *J Am Chem Soc* **2016**, *138*, 313.

(5) Goldsmith, Z. K.; Harshan, A. K.; Gerken, J. B.; Voros, M.; Galli, G.; Stahl, S. S.; Hammes-Schiffer, S. *P Natl Acad Sci USA* **2017**, *114*, 3050.

(6) Trzesniewski, B. J.; Diaz-Morales, O.; Vermaas, D. A.; Longo, A.; Bras, W.; Koper, M. T. M.; Smith, W. A. *J Am Chem Soc* **2015**, *137*, 15112.

(7) Li, N.; Bediako, D. K.; Hadt, R. G.; Hayes, D.; Kempa, T. J.; von Cube, F.; Bell, D. C.; Chen, L. X.; Nocera, D. G. *P Natl Acad Sci USA* **2017**, *114*, 1486.

(8) Fidelsky, V.; Toroker, M. C. *Phys Chem Chem Phys* **2017**, *19*, 7491.

(9) Kresse, G.; Furthmuller, J. *Phys. Rev. B* **1996**, *54*, 11169.

(10) Perdew, J. P.; Burke, K.; Ernzerhof, M. *Phys. Rev. Lett.* **1996**, *77*, 3865.

(11) Won, D. H.; Shin, H.; Koh, J.; Chung, J.; Lee, H. S.; Kim, H.; Woo, S. I. *Angew Chem Int Edit* **2016**, *55*, 9297.

(12) Lim, H. K.; Shin, H.; Goddard, W. A.; Hwang, Y. J.; Min, B. K.; Kim, H. *J Am Chem Soc* **2014**, *136*, 11355.

(13) Shin, H.; Ha, Y.; Kim, H. *J Phys Chem Lett* **2016**, *7*, 4124.

(14) Yook, S.; Shin, H.; Kim, H.; Choi, M. *Chemcatchem* **2014**, *6*, 2836.

(15) Van der Ven, A.; Morgan, D.; Meng, Y. S.; Ceder, G. *J. Electrochem. Soc.* **2006**, *153*, A210.

(16) Trześniewski, B. J.; Diaz-Morales, O.; Vermaas, D. A.; Longo, A.; Bras, W.; Koper, M. T. M.; Smith, W. A. *J. Am. Chem. Soc.* **2015**, *137*, 15112.

(17) Sproviero, E. M.; Gascon, J. A.; McEvoy, J. P.; Brudvig, G. W.; Batista, V. S. *J Am Chem Soc* **2008**, *130*, 6728.

(18) Meyer, T. J.; Huynh, M. H. V.; Thorp, H. H. *Angew Chem Int Edit* **2007**, *46*, 5284.

(19) Ping, Y. and Nielsen, R. J. and Goddard III, W. A. *J. Am. Chem. Soc.* **2017,** *139*, 149

Table of Contents